Polish J. Chem., **78**, 1391–1412 (2004)

Electrochemical Formation and Properties of (Ir+Pb) Oxide*

by A. Piekarska[1], H. Elżanowska[1] and V.I. Birss[2]**

[1]*Department of Chemistry, University of Warsaw, Pasteura 1, 02-093 Warsaw, Poland*
[2]*Department of Chemistry, University of Calgary, Calgary, Alberta, Canada T2N 1N4*

(Received June 7th, 2004)

The incorporation of Pb redox sites into nanoparticulate Ir oxide films has been realized by the initial electrodeposition of Pb metal on Au substrate, followed by Ir metal coating. The amount of Pb was varied according to the conditions of the deposition process, i.e. time, potential and solution used. Nanoparticulate metallic Ir films were obtained via sol-gel (SG) route and the oxidation of the surface was performed electrochemically in sulfuric acid solutions. The amount of Pb incorporated into the oxide film significantly changed the electrochemical response of the mixed oxide. With a relatively large amount of Pb deposit, consisting of under potential deposition (upd) Pb monolayer and Pb clusters, metallic Ir coating is more difficult than on Au and, consequently, only a small amount of Ir oxide is formed by potential cycling of the Au/(Pb+Ir) metallic electrode. The redox kinetics of Ir(III)/Ir(IV) sites, calculated from chronocoulometric data as a diffusional constant $D^{1/2}C$, is diminished. In contrast, with a relatively small amount of Pb present only as clusters on the Au/Pb electrode after potential cycling in sulfuric acid solution, the diffusional kinetics of Ir(III)/Ir(IV) sites is enhanced (7×10^{-7} mol cm^{-2} s$^{-1/2}$ *vs.* 4×10^{-7} mol cm^{-2} s$^{-1/2}$) as compared to Ir oxide. Also, a small negative shift of the prepeak region of the (Ir+Pb) oxide suggests the presence of additional redox process due to incorporation of Pb sites into the oxide structure. When such mixed (Ir+Pb) oxide containing a small amount of Pb is transferred into 1 M KOH solution, the redox processes of Ir and Pb are then more clearly separated and new redox peaks appear negative of Ir oxide peaks at –0.2 V, and also at +0.3 V and +0.9 V, proving the presence of Pb in the oxide. These redox potentials are comparable to the potentials of $Pb_2(Pb_xIr_{2-x})O_{7-y}$ compound obtained thermally and to the redox potentials of Pb electrode in alkaline solutions. The structure of the Pb and Ir deposits and the mixed (Ir+Pb) oxide films was probed using STM imaging. The Pb monolayer (upd) and uniformly distributed Pb clusters ca. 100–150 nm in size were observed on the Au support. The size of metallic Ir nanoparticles is estimated as close to 3–4 nm, increasing to 10–15 nm and 20–30 nm after oxidation of IrO_x and mixed (Ir+Pb) oxide, respectively.

Key words: Pb deposition, Ir metal, Ir oxide, sol-gel, nanoparticulate, thin films, cyclic voltammetry

Hydrous Ir oxide films formed electrochemically have received a great deal of attention over the years, particularly due to their applicability in electrochromic devices [1–3], as electrocatalysts [4–9], interneural stimulating electrodes [10,11], pH electrodes [12–14], cathodes for advanced rechargeable batteries [3,29] and,

---

* Dedicated to Prof. Dr. Z. Galus on the occasion of his 70th birthday.
**Corresponding author. Tel.: (48) 22 822 0211 E-mail address: helzan@chem.uw.edu.pl

recently, as biosensors [15] and supercapacitors [16–18]. Such diverse potential applications of the hydrous Ir oxide prompted the investigations of the electrochemical properties of this oxide, pioneered by Conway's [1,2,5], Gottesfeld's [6] and Burke's [3,19–21] groups and continued later [22–35].

Hydrous electrochemically formed oxides exhibit so called super-nernstian behavior [3,19–35], i.e. higher than 60, usually 70–90 mV/pH potential shift of the main [Ir(IV)/Ir(III)] redox peak with the solution pH. As the amount of H^+ (or OH^-) ions injected/ejected into/from the oxide film is larger than 1 per 1e exchanged, the counterions, either anions in acidic solutions, or cations in basic solutions, have to move in and out of the film to preserve the electroneutrality of the bulk of the oxide. Also, as described by the following equations, the hydration of the oxide may change during the redox processes:

$$\mathrm{Ir(IV)oxide \cdot nH_2O + e^- + xH_3O^+ + yA^-} \longleftrightarrow$$

$$\mathrm{Ir(III)oxide \cdot mH_2O(H_3O^+)_x(A^-)_y + (n-m)H_2O} \quad (1)$$

$$\mathrm{Ir(IV)oxide \cdot nH_2O(OH^-)_x(M+)_y + e^- + mH_2O} \longleftrightarrow$$

$$\mathrm{Ir(III)oxide \cdot (n+m)H_2O + xOH^- + yM^+} \quad (2)$$

The involvement of anions in the redox processes of the Ir oxide films has been demonstrated by the analysis [23] of potassium, lithium and fluoride ion contents of the Ir oxide film [23]. To describe the movement of both the anions and the solvent quantitatively, the QCMB method has been used [27], monitoring the total change of mass of the Ir oxide during the redox processes. The amount of water exchanged in the reaction was calculated from the difference between the total mass change obtained from the QCMB measurements and the mass of cations and anions, calculated according to the pH dependence of the Ir(IV)/Ir(III) redox reaction within the oxide film. An interesting conclusion drawn [27] from the results of these calculations was that the movement of water molecules should be opposite to the movement of ions [equations (1) and (2)].

The hydrous Ir oxide films formed by potential cycling of the metallic Ir electrode can be as thin as a few monolayers, but also very thick, consisting of hundreds of monolayers, when prolonged potential cycling is applied [1–3,19–35]. It is usually assumed that a single monolayer of Ir oxide is equivalent to the charge of *ca*. 0.1 mC cm^{-2} [22–35,36] and the thickest films reach *ca*. 90 mC cm^{-2} (900 monolayers, *ca*. 1 μm thick). As expected, such thick films exhibit slow redox kinetics and reversible CVs can only be obtained at slow sweep rates < 10 mV s^{-1}. Thick films are also prone to aging [28–31], which additionally decreases the rate of the redox processes of Ir sites [31]. For these reasons, the thickest oxides that can be used for practical purposes are only 30 mC cm^{-2} (*ca*. 300 monolayers) [31]. Higher charge densities of Ir oxide with retained fast redox response can be achieved with nanostructured Ir oxide films.

The Ir metal nanoparticulate deposits, 2–3 nm, on Au or Pt support have been obtained [32,33,37] using a sol-gel (SG) method, followed by the electrochemical oxidation of Ir to IrO_x. With each deposition at fast withdrawal rates (240 cm/min), the charge density calculated according to the geometric area is *ca*. 10 mC cm^{-2} and the procedure can be repeated several times, leading to oxide charges of at least 80 mC cm^{-2}. The roughness factor of these nanostructered films is close, however, to 30, and therefore only 2–3 monolayers of the IrO_x film are expected to be deposited. Indeed, SG formed Ir oxide films exhibit a fast kinetic response, typical for thin bulk Ir oxide films [32,33].

The kinetics of diffusion of charge carriers (ions or electrons) through the bulk Ir oxide has been studied in detail for Ir(III)/Ir(IV) redox processes both in the prepeak, A_0/C_0 , and in the main peak, A_1/C_1 regions [31], and the oxidation/reduction to higher oxidation states, Ir(IV)/Ir(V,VI), has also been described [3,19–21,31]. The apparent diffusion constant, $D^{1/2}C$, calculated from chronocoulometric experiments is 2×10^{-7} mol cm^{-2} $s^{-1/2}$ for the A_1 process in the bulk oxide films [31]. Therefore, depending on the oxide thickness, the reaction can be completed in 50–300 miliseconds, *i.e*. it is much faster than the redox processes in most polymeric organic films. The second oxidation step can even be ten times faster [31]. Also, for the nanostructured IrO_x films, fast redox responses are seen, but these are related to the formation of the thin layers rather than to the increase in the diffusion transport through the oxide film.

The kinetic limitation of the Ir(III) to Ir(IV) oxidation is also related to the initial stages of the film oxidation realized for thin oxides in the A_0 prepeak, for which the $D^{1/2}C$ is in the range of 10^{-10} mol cm^{-2} $s^{-1/2}$ [31], *i.e*. it is 2 to 3 orders of magnitude smaller than for the oxidation of the main portion of the Ir oxide in the A_1 region. According to our previous work on the ageing of the Ir oxide films [28–31], the rate of the A_1 process increases when the oxide is already partially oxidized, *i.e*. when the electrode potential is kept positive of the prepeak region. Further improvement of the Ir oxide redox kinetics could be therefore achieved by making changes in the initial stages of Ir(III) oxidation. The incorporation of redox centers with a lower redox potential than Ir(III)/Ir(IV) into the Ir oxide structure could be one of the possible methods used to alter the initial stages of the oxide oxidation process.

We have focused our recent efforts on modifying the properties of the Ir oxide by the formation of mixed oxide films containing Pb as an another metallic center. The choice of Pb as an additional oxide component stems from recent works on the deposition of thin metallic Pb layers [38–40], the redox properties of Pb electrodes [38–43], and also [44] on the properties of the electrodes prepared from oxide compounds containing Ir and Pb, Eu or Sr. Such mixed oxides of known stoichiometric composition are usually prepared by solid state synthesis from stoichiometric mixtures of oxides and carbonates at temperatures as high as 800°C. The oxides are mixed then with carbon and propanol to form pellets that can be used as electrodes [44]. In this work, the (Ir+Pb) oxide electrodes, containing various amounts of Pb, have been formed electrochemically. Both Ir and Pb were deposited as metals on Au support and then these deposits were oxidized electrochemically. No other

compounds were needed to form the mixed oxide electrodes. Each stage of the deposition process, *i.e*. the formation of a upd Pb monolayer, Pb clusters, Ir metal nanoparticles and hybrid oxide nanoparticles, has been monitored using the STM method. It will be shown that, depending on the amount and form of the initial Pb deposit, the presence of Pb in the oxide structure changes the kinetics of the Ir(III)/Ir(IV) redox process in the (Ir+Pb) oxide, resulting in either diminishment or enhancement of the rate of this process.

EXPERIMENTAL

Pb deposition. Pb was deposited on working Au electrodes, *ca*. 0.8 cm^2, in 1 M HNO_3 solution containing 0.5–60 mM Pb^{2+}, either by potential cycling to –0.5 V or potential holding at –0.6 V for varying amounts of time. The Pb coated Au electrode was then transferred to 0.5 M H_2SO_4 and cycled for a few minutes.

Sol-gel method employed for Ir film deposition. The SG solution was prepared as described elsewhere [32,33,38], using a molar ratio of $IrCl_3$ (or $IrCl_3 \cdot 3H_2O$) to Na ethoxide of 3:1, both dissolved in ethanol. The solution was typically refluxed under Ar for *ca*. 2 hrs, then stirred under Ar for *ca*. 20 hrs, and filtered. Au plates (0.84, 0.96 cm^2) were dip-coated by fast withdrawal from the SG solution. The coated electrodes were then heated in air at 100°C for 15 min. For the preparation of multiple coatings, the dip-coating and drying procedures were repeated.

Electrodes, cell, equipment, and chemicals. The working electrodes, Au plates, with or without deposited Pb, were sol-gel coated as described above. In some experiments the working electrodes, *ca*. 0.1 cm^2, constructed from glass-mounted iridium wire (99.9%, Johnson Matthey, 0.5 nn diam.) were used. A Pt gauze counter electrode and a saturated calomel electrode (SCE) were used in conventional three-compartment glass cells. Cyclic voltammetric and chronocoulometric experiments were performed using a computerized electrochemical system, Autolab (Eco Chemie) with software GPES version 4.4. All experiments were carried out at room temperature. All reagents were ACS grade and were used as received.

RESULTS AND DISCUSSION

1. Formation of bulk and nanostructured Ir oxide films. Figure 1 shows a typical cyclic voltammetric (CV) response of an Ir wire metallic electrode cycled in 0.5 M H_2SO_4 at 0.1 V/s in a wide potential range reaching hydrogen evolution at negative potentials and oxygen evolution at positive potentials. Within each cycle, the redox peaks at *ca*. 0.4, 0.7 and 1.2 V increase in size, indicating the formation of the Ir oxide, while the size of the hydrogen adsorption/desorption peaks at *ca*. –0.2 V remain practically the same. The oxide growth is faster at higher sweep rates or when the potential is pulsed at 50 Hz. The set of three Ir oxide peaks, denoted in Fig. 1 as the prepeak, A_0, the main redox peaks, A_1/C_1, and additional peaks seen at high positive potentials, A_2/C_2, represent various oxidation states of Ir sites in the oxide film. Both A_0 and A_1/C_1 processes are related to the oxidation of Ir(III) to Ir(IV) sites and the A_2/C_2 peaks represent oxidation to Ir(V)/Ir(VI). The presence of the hydrogen adsorption/desorption peaks and hydrogen evolution, seen at negative potentials despite the formation of the oxide film, can be explained [1–3] by the full access of the solution to metallic Ir sites through the highly porous, electrochemically formed Ir oxide film.

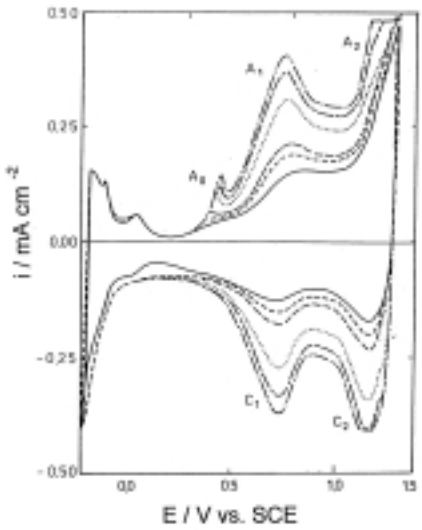

Figure 1. CV response during Ir oxide growth on Ir wire (0.1 cm^2) at 0.1 V/s with continuous cycling between –0.25 and 1.25 V in 0.5 M H_2SO_4 (maximum 12 monolayers).

As shown in our previous work [31,32], the sol-gel (SG) method can be employed to generate nanoparticulate Ir oxide films. The methodology used involves a two-step process (CVs shown in Fig. 2). First, a layer of metallic Ir is deposited (solid lines), and then metallic Ir is electrochemically oxidized to Ir oxide (dotted lines).

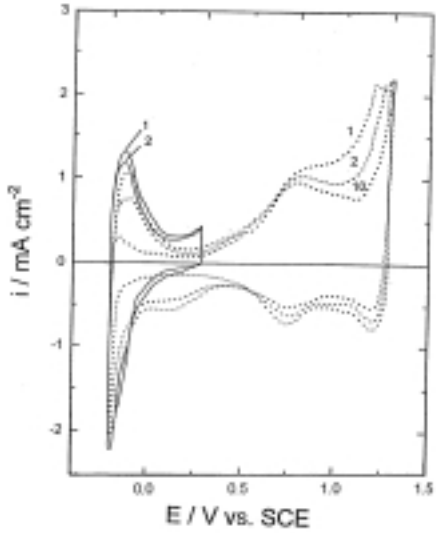

Figure 2. CV response of SG-formed Ir film on Pt foil (0.6 cm^2) at 0.02 V/s in 0.5 M H_2SO_4 in the first and second potential cycles to 0.25 V (solid lines) and in the first, second and tenth cycle to 1.25 V (dashed lines). Ir deposit dried for 15 min at 190°C.

If, in cyclic voltammetry, the electrode potential is kept below 0.3 V *vs*. SCE in 0.5 M H_2SO_4 (solid lines in Fig. 2) to avoid Ir oxidation, the hydrogen adsorption/desorption peaks remain essentially the same with potential cycling. However, extending the positive potential limit to 1.25 V (dotted lines) results in a gradual decrease of the hydrogen peaks with potential cycling in a 1st, 2nd, and 10th cycle. Finally, the electrode response in the hydrogen region is typical for the Pt support used for Ir nanoparticle deposition, reflecting the Pt area exposed to the solution and available for hydrogen adsorption. Also, the Ir metal is converted to Ir oxide, as seen by the appearance of the redox peaks at *ca*. 0.75 V (Fig. 2, dotted lines).

When Au is used as a support for the Ir deposition, the hydrogen adsorption/desorption processes are not seen and only hydrogen evolution is observed starting from *ca*. –0.3 V (curve 1 in Fig. 3). Therefore, the hydrogen peaks seen after SG deposition of metallic Ir (curve 2) reflect only the hydrogen adsorption/desorption on Ir deposit and can easily be used to estimate the roughness factor of the Ir deposit. Assuming that only 65% of the surface is covered with H (65% of 0.21 mC/cm^2, ref. 38), the calculated surface area is *ca*. 30 times higher than the geometric area of the supporting Au electrode. Such a high roughness factor of the Ir deposited via the SG route, is a consequence of the microstructure of the deposit, consisting of nanoparticles of *ca*. 2–3 nm, as estimated before using the SEM [32,33] and STM [37] methods.

The STM images of the metallic Ir and Ir oxide are shown in Figs. 4a, 4b and 4c, 4d, respectively. After electrochemical oxidation by potential cycling, some of the metallic Ir nanoparticles (2–3 nm) fuse to form *ca*. 10–15 nm oxide aggregates. These aggregates retain, however, the 2–3 nm nanoparticulate structure and are only seen at some parts of the electrode. Therefore, the estimation of the roughness factor of nanoparticulate Ir oxide deposit from the charge under the hydrogen adsorption/desorption peaks on metallic Ir seems to be justified.

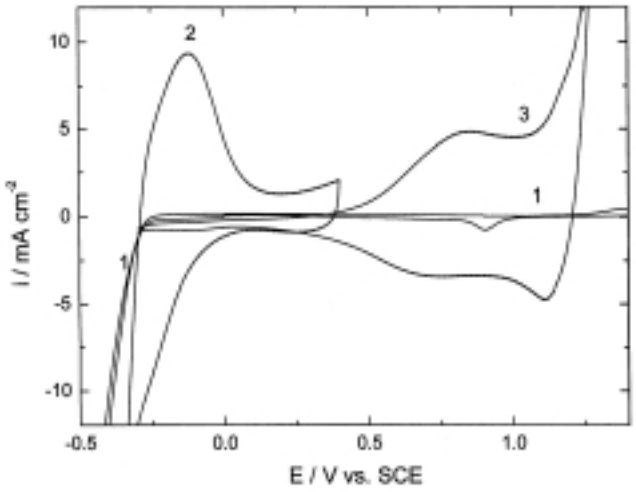

Figure 3. CV response at 0.1 V/s of Au foil (0.84 cm^2) electrode in 0.5 M H_2SO_4 before (1) and after coverage with SG formed Ir film; continuous potential cycling up to 0.3 V (2) and 1.25 V (3). Ir deposit dried for 15 min at 100°C. Curve (3) depicts the response of [Au/IrO_x] electrode.

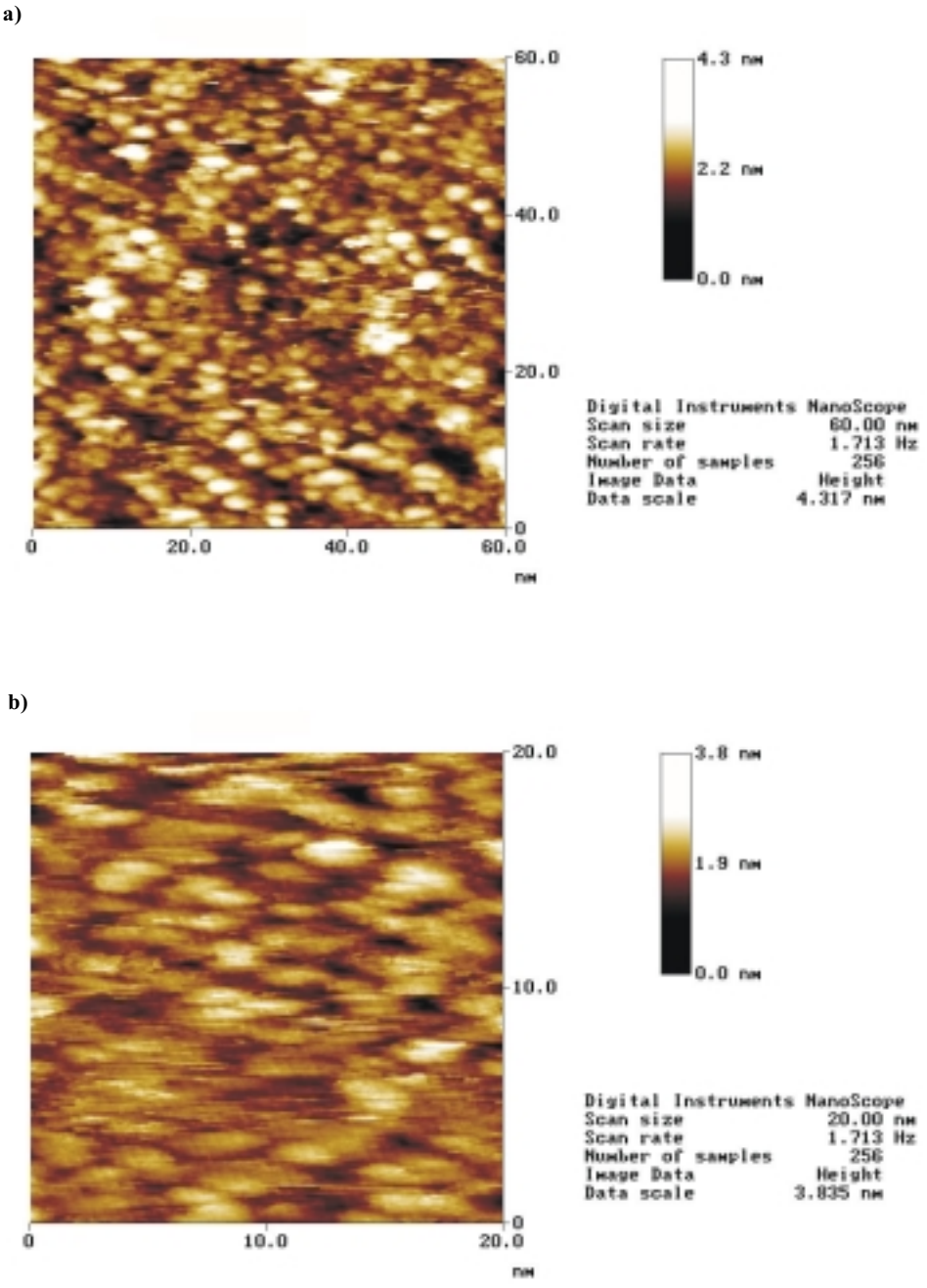

Figure 4. STM image of polycrystalline Au covered by SG derived Ir before (a, b), and after oxidation to IrOx (c, d).

c)

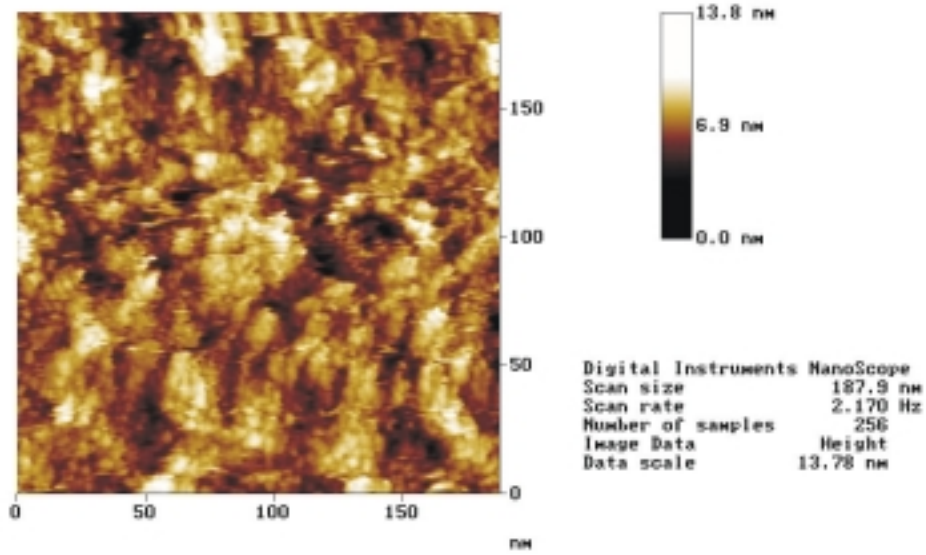

d)

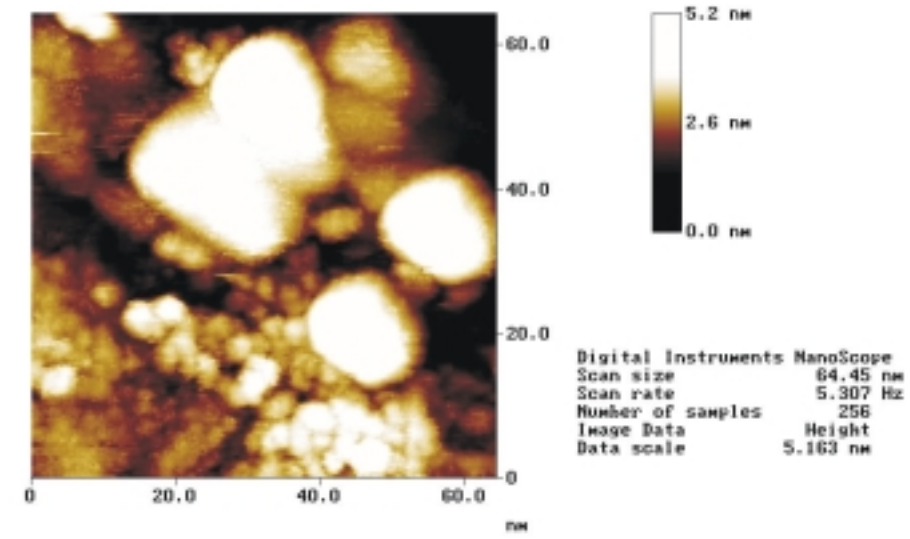

Figure 4 (continuation).

2. Formation of (Ir + Pb) oxide nanoparticles. The mixed (Ir+Pb) oxide nanoparticles were formed using a three step procedure: (1) deposition of Pb on Au, both as an underpotential deposition and as Pb clusters formed at potentials more negative than the standard Pb(II)/Pb potential, (2) coverage of Au/Pb electrode with Ir metal nanoparticles, using a SG method, and (3) electrochemical oxidation of the nanoparticulate metallic Au/Pb/Ir electrode to the oxide. Each step has been monitored electrochemically, using cyclic voltammetry, and microscopically, by STM imaging.

2.1. Deposition of Pb on Au [Au/Pb]. The amount of Pb deposited on Au support can be varied by changing the concentration of Pb(II) in solution as well as the deposition time and potential. In this section, a typical example of Pb deposition as a upd Pb monolayer and clusters formed on Au will be described in detail.

Figure 5 shows a cyclic voltammogram of the Au electrode at 0.1 V/s obtained in 1 M HNO_3 solution (curve 1) and in the same solution containing 2 mM Pb(II) (curves 2 and 3). Curve 2 depicts the electrode response in the first potential cycle and curve 3 shows the CV obtained after potential holding at –0.6 V for 150 s. At negative potentials, the hydrogen evolution, usually seen at Au electrode close to –0.3 V (curve 1), is not visible even up to –0.6 V due to the deposition of Pb on the Au electrode (curves 2 and 3). As expected [41,43], the initial potential cycling (curve 2) in the presence of Pb ions leads to underpotential deposition of lead in the cathodic sweep, and the subsequent dissolution of this Pb deposit in the anodic sweep, both occuring in the potential range from *ca.* 0.1 V to –0.5 V. Also, a very small amount of a permanent Pb deposit can be formed (curve 2) as the potential is cycled up to –0.6 V, *i.e.* close to the standard potential of a Pb(II)/Pb redox couple [$E^0(Pb^{2+}/Pb) = 0.61$ V]. A sharp Pb(II) reduction peak and subsequent oxidation peak, both close to –0.55 V,

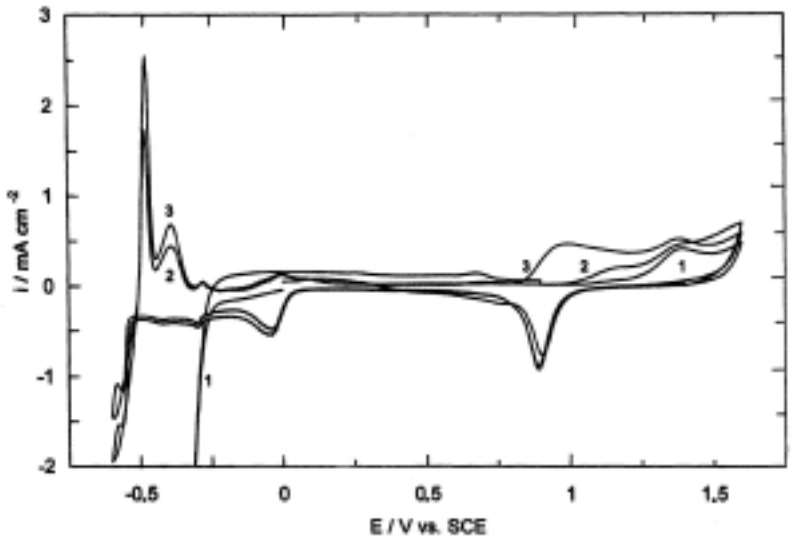

Figure 5. CV response at 0.1 V/s of Au foil (0.84 cm^2) electrode in 1 M HNO_3 (1) , in 2 mM Pb^{2+}/1 M HNO_3 in the first potential scan (2) and after potential holding at –0.6 V for 150 s (3).

seen in Fig. 5 (curve 2) are typical [38–41] for Pb deposition and oxidation to PbO. At positive potentials, the Au oxide formation observed at *ca*. 1.3 V, and its reduction at *ca*. 0.9 V, both remain only slightly altered (curve 2), suggesting that the Pb deposit is practically removed with cycling to high positive potentials.

To form a permanent Pb deposit, seen as a darkening of the Au surface, the potential of the Au electrode has to be held at –0.6 V for at least a few minutes (*e.g.* 150 s). This process is accompanied by a significant negative shift in the Au oxidation peak from 1.3 V to *ca*. 0.85 V (curve 3 in Fig. 5). Since the upd Pb deposit should be dissolved at potentials more positive than +0.2V [41,43], the formation of a permanent Pb deposit should rather be responsible for the changes in the Au oxidation.

The results presented above are in agreement with the findings presented in earlier publications [38–40] regarding the deposition of Pb on various supports, *e.g.* on Pt and reticulated vitreous carbon (RVC). Typically, a micron thick Pb deposit would require 20–30 min of potential holding [38–40] and therefore only a relatively small, but stable amount of Pb could be deposited in this work at 150 s. If, however, after deposition, the Au electrode with a certain amount of Pb is removed from the solution at –0.6 V, both permanent and upd Pb deposits could be present on the electrode surface.

The STM image of the polycrystalline Au electrode taken after Pb deposition by potential holding at –0.6 V for 150 s is shown in Fig. 6c and can be compared with the image of pure polycrystalline Au shown in Fig. 6a, both at high magnification (15 μm). The Pb deposits are seen on Au as fairly uniform clusters *ca*. 100–50 nm in size. One of the clusters is presented more clearly at lower magnification (1 μm) in Fig. 6d. Also, the upd Pb deposit, uniformly covering the Au surface, seems to be visible in Fig. 6d.

2.2. SG formed Ir metal films on Au/Pb electrodes [Au/(Ir+Pb)]. To form a mixed Pb and Ir deposit, a sol-gel method has been employed to form Ir metallic nanoparticles on the Au electrode previously covered with Pb clusters. An Ir sol was deposited on Au/Pb electrode using the constant withdrawal rate and then the sample was heated at 100°C for 15 min to form an Ir film. The same procedure has been used previously to form nanoparticulate Ir deposits on various supports such as Au, Pt and GC [32,33 and 37]. The Au support has been chosen in this work as the hydrogen adsorption/desorption peaks are absent on Au electrodes and, therefore, their presence can only be attributed to Ir metal deposition on this support and reflects the electrode area covered by Ir deposit (see also Figs. 2 and 3).

Figure 7 shows the cyclic voltammograms at 0.1 V/s in 0.5 M H_2SO_4 of the Au electrode covered first with Pb (Au/Pb, curve 1) and then with Ir metal (Au/(Ir+Pb), curve 2). The Au electrode was covered with Pb by potential holding at –0.6 V for 150 s in 1 M HNO_3 and withdrawn from the solution at –0.6 V, so both upd and permanent Pb deposits should be present on the electrode as shown by STM images in Figs. 6a–6d. The SG derived Ir metallic film was placed on top of these deposits and the Au/(Ir+Pb) electrode was transferred to 0.5 M H_2SO_4 (curve 2 in Fig. 7).

a)

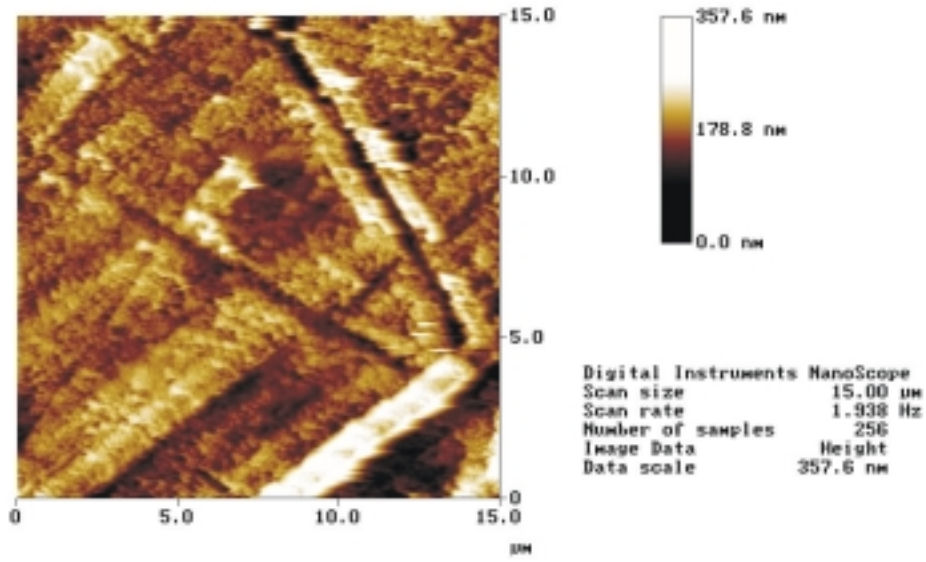

b)

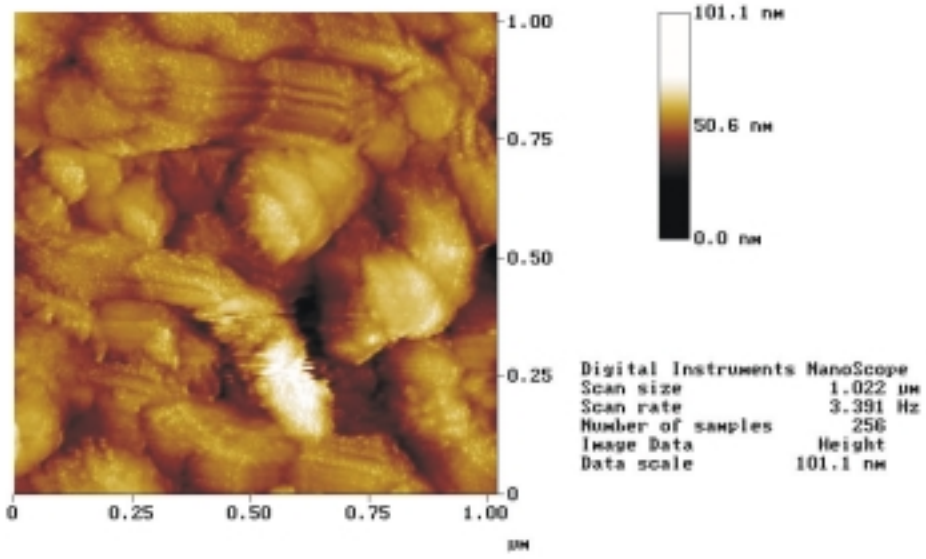

Figure 6. STM image of polycrystalline Au before (a, b) and after (c, d) electrochemical deposition of Pb at –0.6 V for 150 s in 1 M HNO_3.

c)

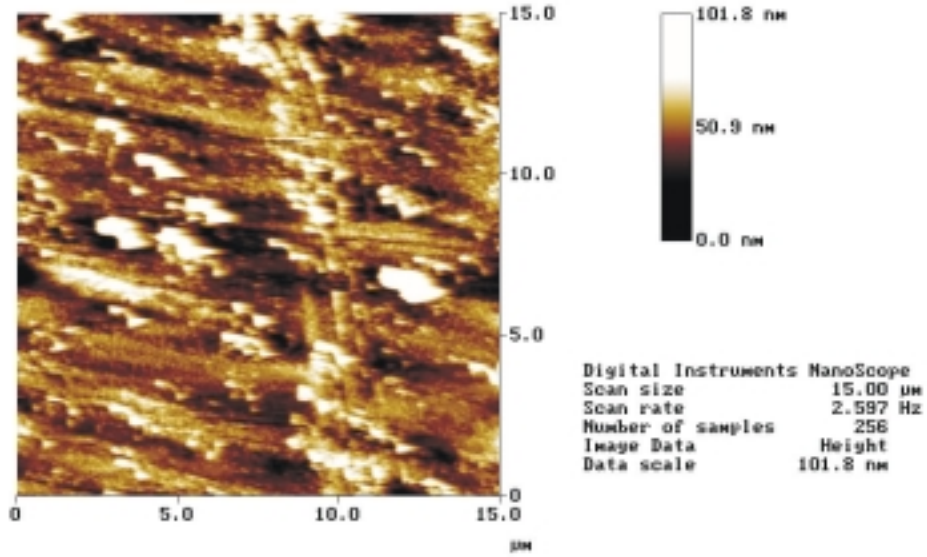

d)

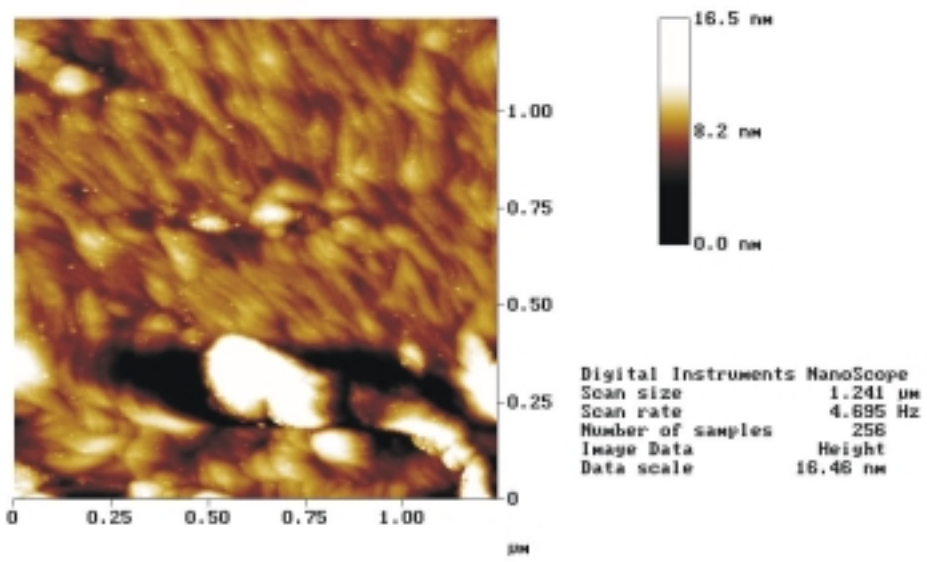

Figure 6 (continuation).

The response of the Au electrode covered only with Pb and transferred to sulfuric acid solution is shown in Fig. 7 (curve 1) to show that even after potential cycling in the solution without Pb^{2+}, the Pb deposit is still present on the Au surface. The upd Pb layer is not expected to be seen, though, it should be dissolved with cycling to potentials more positive than 0.2 V [41]. The presence of Pb deposit on Au prevents the evolution of hydrogen on the electrode surface at least up to –0.5 V. On pure Au, the reduction of hydrogen would already be seen at *ca.* –0.3 V (see curve 1 in Fig. 3), while the evolution of H_2 on metallic Pb is expected at –1.0 V [38]. These results prove that, in 0.5 M H_2SO_4 solution, the Pb deposit, not even covered by metallic Ir, is still kept on the electrode, probably in the form of oxide and sulfate.

After Ir metal deposition, the hydrogen adsorption/desorption peaks, typical for Ir metallic surface, are clearly seen in the potential range from 0 to –0.3 V (curve 2 in Fig. 7). This result is expected here, as a major part of the surface is now covered with Ir. However, Pb should also be present on the electrode surface underneath the Ir metallic film, as even pure Pb deposit is stable in sulfuric acid (curve 1 in Fig. 7). It should also be noted that the oxidation of Ir to IrO_x is prevented [32,33] by restricting the potential cycling to 0.4 V (curve 2 in Fig. 7).

The STM image of the Au/(Ir+Pb) electrode (Fig. 8b) is similar to the one taken for pure Au electrode covered with Ir nanoparticles (3–5 nm) and shown before in Fig. 4a (at high magnifications 100 nm and 60 nm, respectively). At lower magnification (1 μm), the deposits of *ca*. 200 nm are seen as bright spots in Fig. 8a, suggesting that the Pb clusters remain on the surface. Some of these clusters might be removed, though, as dark spots, possibly the holes in the Au surface, are also seen in this figure. Such dark spots are typical for the Au electrode that was cleaned

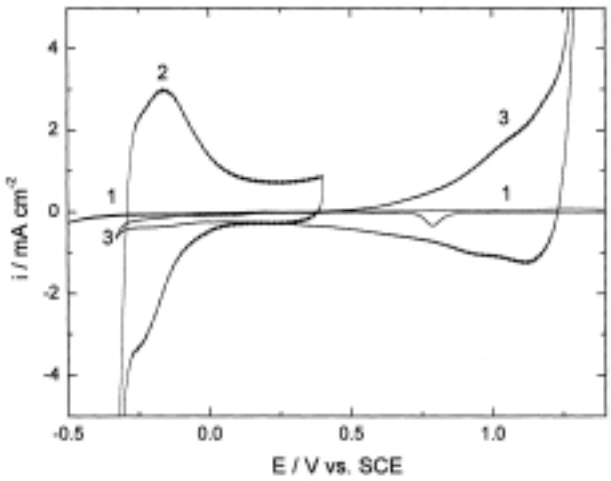

Figure 7. CV response at 0.1 V/s of Au foil (0.84 cm2) electrode in 0.5 M H_2SO_4 after Pb deposition from 2 mM Pb^{2+}/1 M HNO_3 solution (1), followed by coverage with SG formed Ir film at constant withdrawal rate (2), and electrochemical oxidation by potential cycling at 0.1 V/s from –0.3 to 1.25 V (3). Pb deposited by potential holding at –0.6 V for 150 s. Ir deposit dried for 15 min at 100°C. Curve (3) depicts the CV the response of [Au/(Pb+Ir) oxide (1)] electrode.

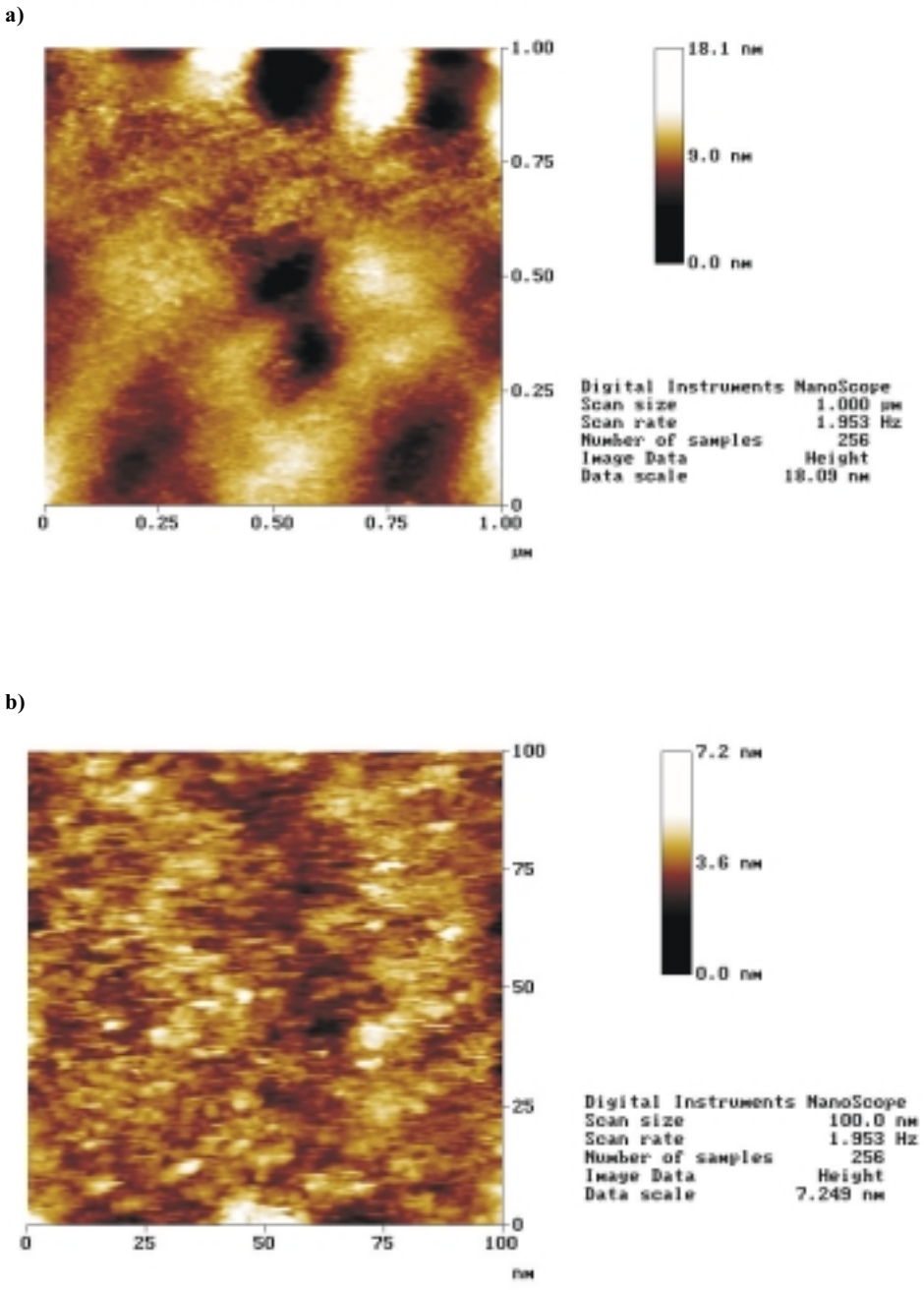

Figure 8. STM image of SG derived nanoparticulate metallic Ir deposited on Au/Pb electrode.

after Pb deposition by sonication in hydrogen peroxide solution, indicating probably a rough Au surface remained after removal of the Pb cluster. When the parts of the surface between the clusters are examined at higher magnification (60 nm), the STM image shows that the electrode is covered uniformly with 2–3 nm nanoparticles, presumably metallic Ir nanoparticles.

2.3. Oxidation of Au/(Ir+Pb) electrode [Au/(Ir+Pb) oxide]. The oxidation of metallic deposits on Au/(Ir+Pb) electrode has been realized using potential cycling, a procedure typically used [32,33] to form an Ir oxide. The potential was cycled in a wide range reaching hydrogen and oxygen evolution regions at negative and positive potential limits, respectively. It can be seen in Fig. 7 that the hydrogen absorption/desorption peaks diminish as Ir is transformed to IrO_x (curve 3 *vs*. curve 2) and the hydrogen evolution occurs at *ca*. –0.3 V now, *i.e.*, at the potential typical for the Au support (see also curve 1 in Fig. 3). For IrO_x [section 1, refs. 32,33], such change in hydrogen absorption/evolution is indicative of the oxidation of metallic Ir sites within the Ir deposit. It can be anticipated therefore that also metallic Pb is now (Fig. 7, curve 3) in the oxidized state, forming a mixed (Ir+Pb) oxide film.

The presence of lead in the hybrid (Ir+Pb) oxide is also supported by the STM images of the electrode surface. The STM images of the Au/(Pb+Ir) electrode oxidized to Au/(Ir+Pb) oxide (Figs. 9a–9b) show *ca*. 20–30 nm clusters consisting of 2–3 nm units, larger than usually obtained for pure Ir oxide deposits (Fig. 4d, *ca*. 10–15 nm). Also, the surface is rougher than seen for IrO_x, suggesting that the initial Pb deposits of *ca*. 100–150 nm are incorporated into the oxide structure.

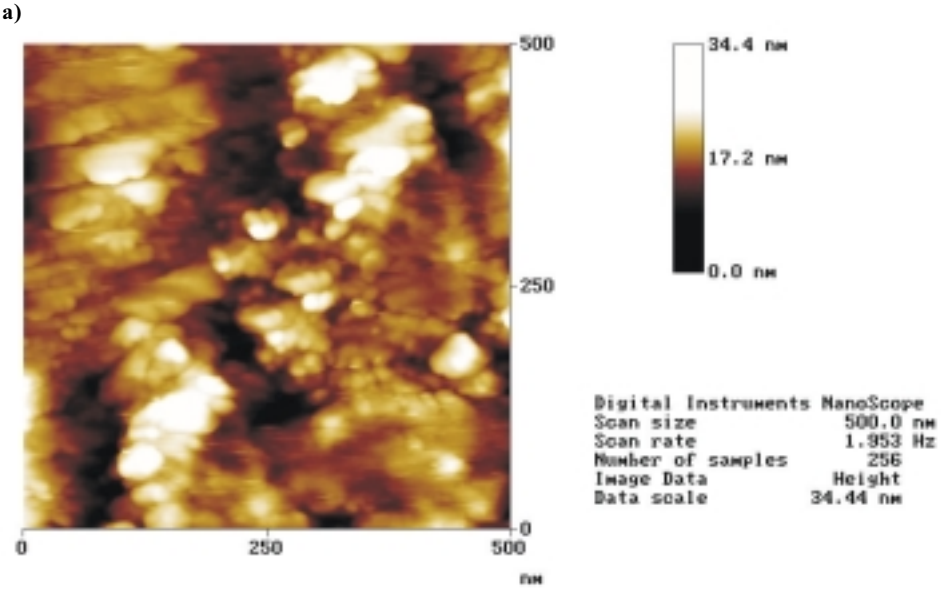

Figure 9. STM image of SG derived nanoparticulate metallic Ir deposited on Au/Pb electrode and oxidized electrochemically to the oxide.

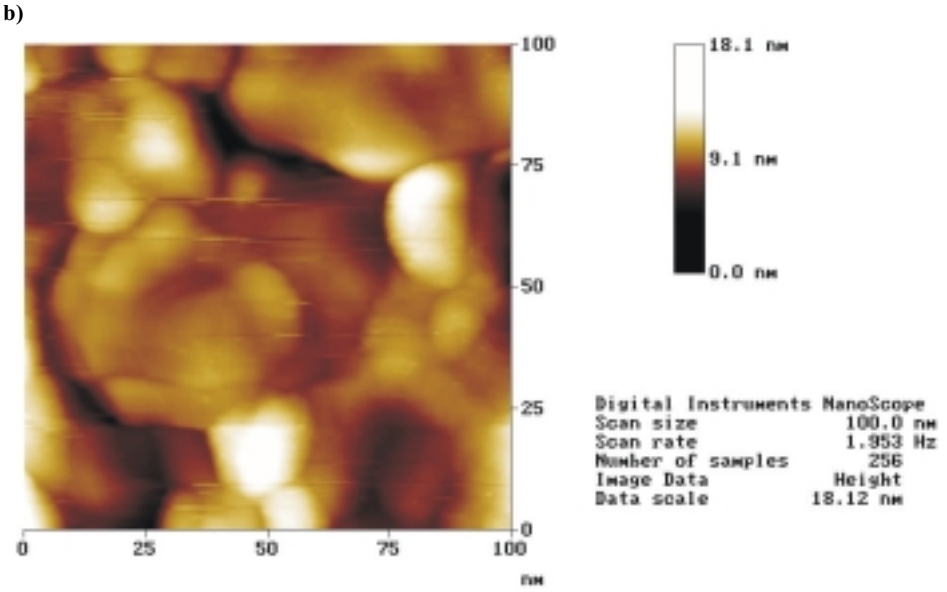

Figure 9. (continuation).

Another argument for the presence of Pb in the oxide is that the kinetics of Ir(III)/Ir(IV) redox reaction (Fig. 7, curve 3) is clearly slower than observed before (Fig. 3, curve 3) for pure IrO_x. Now, the main Ir(III)/Ir(IV) oxidation peak in a CV experiment at 0.1 V/s is shifted from *ca*. 0.7 V to at least 0.85 V merging with the peak of Ir(IV) to Ir(V,VI) oxidation. The reduction peaks are smaller than the expected symmetrical oxidation peaks and the reduction peak potentials are not clearly defined.

3. Properties of mixed (Ir+Pb) oxide films. The properties of mixed (Ir+Pb) oxide films depend strongly on the amount of Pb in the oxide film. As discussed in the previous section, the initial Pb deposit consisting of both upd and permanent Pb deposits of *ca*. 100–150 nm clusters covered later by Ir nanoparticles (see STM images in Figs. 8c, 8d), results in the decrease of the rate of Ir(III)/Ir(IV) oxidation in the mixed film. In contrast, it will be shown in this section that the initial Pb deposit in the form of a permanent Pb deposit only, *i.e*. with no upd Pb deposit present, placed on the Au electrode before the Ir film, results in the increase of the rate of Ir(III)/Ir(IV) oxidation in the mixed film.

3.1. Changes of redox kinetics with the amount of Pb in the mixed oxide. Figure 10 shows the CV of a mixed Ir+Pb oxide formed using the same procedure as described before (section 2), but this time, prior to the SG deposition of a metallic Ir film, the Au electrode with a Pb deposit has been cycled in 0.5 M H_2SO_4 for a few minutes. In this experiment no Pb(II) ions are present in the solution, so further

deposition of Pb is not possible. The upd formed Pb should be dissolved as the potential is cycled positively of 0.2 V [41], but the permanently deposited Pb clusters should remain, at least partly, on the Au surface, either as Pb oxide or sulfate [38–40].

From the comparison of the potential of hydrogen evolution in Figs. 10 and 7, it can be seen that after potential cycling in 0.5 M H_2SO_4 solution, the amount of Pb on the surface is clearly smaller in Fig. 10 than shown before in Fig. 7 (section 2.2). In Fig. 10, the hydrogen evolution is already seen at *ca.* –0.35 V at Au/Pb surface (curve 1) and was not observed before up to –0.5 V (Fig. 7, curve 1). The Pb deposit is still present, however; otherwise the hydrogen evolution would have been seen at pure Au surface at *ca.* –0.3 V (see Fig. 2, curve 1, section 1). The peak height of the hydrogen desorption peak is higher than with previous Pb deposits (Fig. 7), but still smaller than without the Pb deposit (peak heights of *ca.* 7, 3 and 9 mA cm^{-2} in Figs. 10, 7 and 3, respectively). No STM images are shown for the Au/Pb samples cycled in sulfuric acid before Ir deposition, as the amount of Pb left on the surface depends strongly on the conditions of the experiment. The presence of Pb on Au in a particular sample can easily be monitored by the onset of hydrogen evolution on the remaining Au sites on the Au/Pb surface.

Contrary to the case of the deposition of metallic Ir without prior cycling of the Au/Pb electrode in 0.5 M H_2SO_4 (Fig. 7), the amount of Ir deposited now (Fig. 11) is similar to the amount usually obtained for pure Au surfaces with *ca.* 5 mA cm^{-2} peak height for the Ir(III)/Ir(IV) CV peak. Also, the Ir(III)/Ir(IV) redox peaks are symmetrical at 0.1 V/s, indicating a fast redox process, faster than for a mixed Ir+Pb oxide prepared without the treatment in 0.5 M H_2SO_4. In fact, the Ir(III) to Ir(IV) oxidation

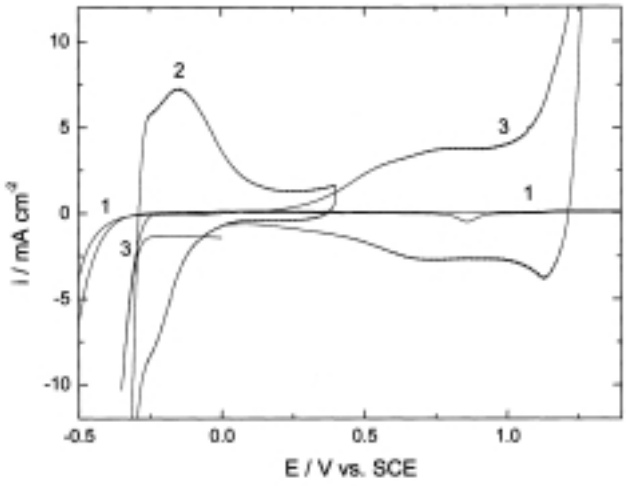

Figure 10. CV response at 0.1 V/s of Au foil (0.84 cm^2) electrode in 0.5 M H_2SO_4 after Pb deposition from 2 mM Pb^{2+}/1 M HNO_3 solution and additional potential cycling in 0.5 M H_2SO_4 (1), followed by SG-formed Ir film at constant withdrawal rate (2), and electrochemical oxidation by potential cycling at 0.1 V/s from –0.3 to 1.25 V (3). Pb deposited by potential holding at –0.6 V for 150 s. Ir deposit dried for 15 min at 100°C. Curve (3) depicts the CV response of [Au/(Ir+Pb) oxide (2)] electrode.

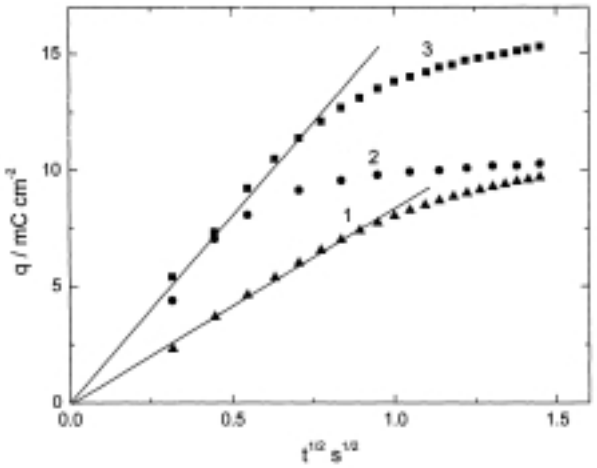

Figure 11. $q/t^{1/2}$ plots for the anodic step from 0.4 V to 0.75 V in 0.5 M H_2SO_4 for SG-formed Ir oxide on Au foil (0.84 cm^2) (1) and mixed (Ir+Pb) oxides (2, 3). Plots 1–3 refer to the following electrodes: (1) [Au/IrOx], see CV in Fig. 3, curve 3, (2) [Au/(Ir+Pb) oxide (2)], see CV in Fig. 10, curve 3, and (3) [Au/(Ir+Pb) oxide (3)], formed by additional SG metallic Ir film added to [Au/(Ir+Pb) oxide (2)], CV not shown.

in the mixed film is even faster than observed for pure Ir oxide. In a chronocoulometric experiment, the slope of q *vs*. $t^{1/2}$ is almost 2 times higher for mixed *vs*. pure oxide showing the same difference in the apparent diffusion constants $D^{1/2}C$ for these oxides (Fig. 11), calculated from the Cottrell equation [31]:

$$q = Q/A = 2nFD^{1/2}\, C\, t^{1/2}\, \pi^{-1/2} \qquad (3)$$

where q is the charge density, D is the diffusion coefficient (cm^2/s) and C is the concentration (mol/cm^3); all other symbols have their usual meaning.

Table 1 summarizes the $D^{1/2}C$ values obtained from the chronocoulometric experiments (equation 3) performed using various types of Ir oxides with and without the addition of Pb. The potential step used was from 0.4 V to 0.75 V, a typical condition for the Ir(III)/Ir(IV) oxidation process. For the sake of comparison, the $D^{1/2}C$ value for the bulk Ir oxide formed on Ir wire (2.0×10^{-7} mol cm^{-2} $s^{-1/2}$, ref. 31) was added in Table 1.

Table 1. Diffusion constants, $D^{1/2}C$, for oxidation process of Ir oxide in 0.5 M H_2SO_4.

Electrode	$D^{1/2}C$ [mol cm^{-2} $s^{-1/2}$]$^{\#}$
IrO_x on Ir wire	2.0×10^{-7} [ref. 31]
[Au/IrO_x]*	4.2×10^{-7}
[Au/(Pb+Ir) oxide (1)]**	1.2×10^{-7}
[Au/(Pb+Ir) oxide (2)]***	7.2×10^{-7}
[Au/(Pb+Ir) oxide (3)]****	8.1×10^{-7}

$^{\#}$ potential step from 0.4 V to 0.75 V; * see Fig. 3; ** see Fig. 7; *** see Fig. 10; **** formed by additional SG metallic Ir film added to [Au/(Ir+Pb) oxide (2)], CV not shown, see text (section 3.1.).

The apparent diffusion constants for the nanoparticulate Ir oxide films are higher than for bulk films, but they only differ by a factor of *ca*. 2, instead of *ca*. 16 expected if the roughness factor of the electrode is taken into account (2 [36] and 32 [32]). Even if the roughness of the electrode is overestimated, for instance due to some dissolution of the metallic Ir during oxide formation (Fig. 2) and due to aggregation of 2–3 nm metallic nanoparticles into 10–15 nm oxide particles, the rate of the A_1 redox process within the oxide film seems to be slower or, at most, comparable to the bulk oxide. Therefore, no net gain in the diffusion constant is seen in nanoparticulate oxide deposits.

With the addition of Pb in a form of a upd layer and Pb clusters (Figs. 7 and 8, [Au/(Ir+Pb) oxide (1)] in Table 1), the diffusion through the oxide film to the Au support is hindered even more, probably due to difficulties in the attachment of metallic Ir to the Pb deposit, in particular to the upd layer. When this upd Pb monolayer is removed by potential cycling in sulfuric acid solution, then the amount of metallic Ir and IrO_x formed is comparable to the amount usually obtained on the Au support (Fig. 10 *vs*. Fig. 3). The incorporation of Pb under such conditions leads to the enhancement of the redox kinetics of the hybrid oxide, as seen by the increase of the apparent diffusion constant in Table 1 from 4.2×10^{-7} mol cm^{-2} $s^{-1/2}$ to 7.2×10^{-7} mol cm^{-2} $s^{-1/2}$ (Fig. 11, [Au/(Ir+Pb)oxide (2)]). It should also be noted that further coverage of the mixed (Ir+Pb) electrode with another layer of metallic Ir followed by its oxidation, does not change the diffusion constant significantly (Fig. 11, [Au/(Ir+Pb)oxide (3)], 8.1×10^{-7} mol cm^{-2} $s^{-1/2}$).

The increased rate of the Ir oxide Ir(III)/Ir(IV) redox process in the presence of a small amount of permanently deposited Pb in the oxide film seems to be related to the changes of the oxide response in the prepeak region, *i.e.* at potentials less positive than the main A_1 peak [(Ir(III)/Ir(IV)] of pure IrO_x (see Fig. 1). For the hybrid oxide, the A_0 prepeak is shifted positively by *ca*. 70 mV, while the main peak is visible at the same potential of 0.75 V for both oxides (not shown). Such shift in the prepeak region had been previously reported for the unaged *vs*. aged Ir oxide [31] and was related to the presence of the Ir sites, presumably closer to the electrode surface, which are oxidized first when the oxide is transformed from nonconducting Ir(III) to conducting Ir(IV). The positive shift of the A_0 prepeak had been related before [31] to the increase of the rate of the main redox process in the Ir oxide film. With the addition of Pb redox sites, it can be anticipated that the Pb sites are oxidized first, thus enabling the Ir sites to be oxidized at a faster rate in an already partly conductive oxide.

3.2. Evidence for the presence of Pb in the mixed (Ir+Pb) oxide in 1 M KOH. In alkaline solutions, the difference between the CV response of the Pb and Ir sites of the mixed (Ir+Pb) oxide could be seen due to the fact that the potentials of the redox processes of these two elements might be shifted differently with the solution pH. Such a shift would be related to various amounts of counter ions needed to balance the charge of each of the redox sites within the hybrid oxide film [see equation (1)]. Indeed, when the mixed (Ir+Pb) oxide, cycled before in sulfuric acid solution (Fig. 10), is transferred to 1 M NaOH (Fig. 12), except for the overall loss of charge, three additional redox peaks could be noticed, related presumably to the presence of Pb sites in the mixed oxide.

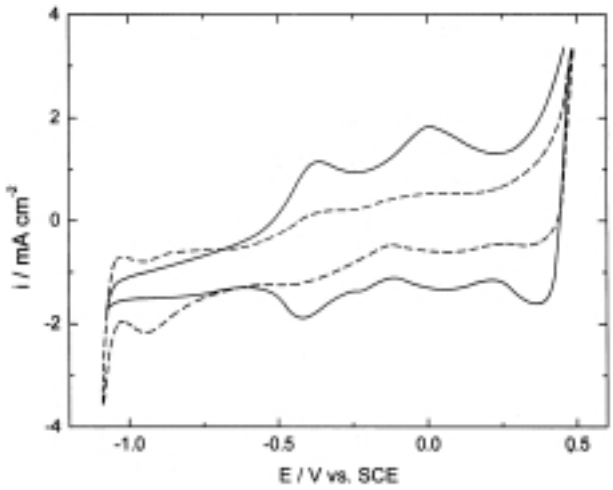

Figure 12. CV response of Au foil (0.84 cm^2) electrode at 0.1 V/s in 1 M KOH after coverage with SG formed IrO_x film with (dotted line) and without (solid line) previously deposited Pb. The oxides were formed as shown in Figs. 3 and 10, respectively.

In Fig. 12, the CV responses are shown for both mixed (Ir+Pb) oxide (dotted line) and Ir oxide (solid line). It can clearly be seen form this figure that the incorporation of Pb is accompanied by the appearance (dotted line) of an additional reduction peak at *ca.* –0.9 V. i.e. at potentials less positive than all the Ir redox peaks (solid line). Also, the redox peaks of Ir, A_1/C_1 and A_2/C_2 merge in the hybrid oxide (dotted line) as compared to IrO_x (solid line) and, therefore, the presence of new redox states at positive potentials close to –0.2 V can be suggested. Moreover, the increase of the oxidation current at high positive potentials at *ca.* +0.3 V is detected in the mixed oxide as compared to IrO_x. The position of the three additional peaks, at –0.9, –0.2 and +0.3 V appearing in the mixed oxide would be in agreement with the potentials of the PbO_2 reduction [(Pb(IV)/Pb(II) at –0.9 V], PbO oxidation [Pb(II)/Pb(III) at –0.2 V] and PbO_2 formation [Pb(III)/Pb(II) at *ca.* +0.3 V] reported in the studies of Pb [42] and Pt/Pb [38] electrodes in alkaline solutions, thus confirming the presence of Pb in the mixed (Ir+Pb) oxides studied in this work. Also, the $Pb_2(Pb_xIr_{2-x})O_{7-y}$ oxide, prepared using solid state synthesis [44], is oxidized and reduced in 1 M KOH at potentials similar to those shown in Fig. 12. Only in the oxides prepared by solid state synthesis [44], the Ir redox peaks, A_1/C_1 and A_2/C_2 are more separated, suggesting the presence of a smaller amount of the Pb or a different distribution of various Pb redox sites in that oxide.

CONCLUSIONS

The mixed (Ir+Pb) oxides have been prepared on Au substrate using a three-step procedure: electrochemical deposition of metallic Pb (1), sol-gel formation of Ir metal (2), and electrochemical oxidation of Ir+Pb surface to the oxide (3). The sizes of nanoparticulate metallic deposits have been estimated as *ca.* 100–150 nm for Pb and *ca.* 2–3 nm for Ir, using STM imaging. The mixed (Ir+Pb) oxide films tend to form aggregates of nanoparticles of *ca.* 20–30 nm, while for Ir oxide films these aggregates are smaller, *ca*. 10–15 nm. The diffusional kinetics of the hybrid films significantly depends on the amount of Pb deposited and on the treatment of the Pb deposit in sulfuric acid solutions. Only the mixed (Ir+Pb) oxides obtained with a relatively small amount of Pb clusters and no upd Pb deposits, exhibit the increase, from 4×10^{-7} mol cm^{-2} s$^{-1/2}$ to 7×10^{-7} mol cm^{-2} s$^{-1/2}$, of the diffusional kinetics of the Ir sites. The presence of Pb in the hybrid films is confirmed by the appearance of additional redox peaks at potentials –0.9, –0.2 and +0.3 V, as obtained in alkaline solutions for the mixed (Ir+Pb) oxide.

Acknowledgments

This work was supported by the Polish State Committee for Scientific Research (KBN), under Grant 3T09A 09313. The assistance of Albin Wisniewski with the STM measurements is greately appreciated.

REFERENCES

1. Conway B.E. and Mozota J., *Electrochim. Acta*, **28**, 9 (1983).
2. Mozota J. and Conway B.E., *Electrochim. Acta*, **28**, 1 (1983).
3. Burke L.D. and Whelan D.P., *J. Electroanal. Chem.*, **124**, 333 (1981).
4. Hefny M.M. and Abdel-Wanees S., *Electrochim. Acta*, **41**, 1119 (1996).
5. Mozota J. and Conway B., *J. Electrochem. Soc.*, **128**, 2124 (1981).
6. Gottesfeld S. and Srinivassan S., *J. Electroanal. Chem.*, **86**, 89 (1978).
7. Nahor G.S., Hapiot H., Neta P. and Harriman A., *J. Phys. Chem.*, **95**, 95 (1991).
8. Pauporte Th., Andolfato F. and Durrand R., *Electrochim. Acta*, **45**, 431 (1999).
9. Trassatti S., *Interfacial Electrochemistry of Conductive Oxides for Electrocatalysis*, in "Interfacial Electrochemistry. Theory, Experiment, and Applications", ed. A. Wieckowski, Marcel Dekker, Inc., 1999, p. 769.
10. Roblee L.S., Lefko J.I. and Brummer S.B., *J. Electrochem. Soc.*, **130**, 731 (1983).
11. Ballestrasse C.L., Ruggeri R.T. and Beck T., *Ann. Biomed. Eng.*, **13**, 405 (1985).
12. Hitchman M.L. and Ramamathan S., *Analyst*, **113**, 35 (1998).
13. Kinlen P.J., Heider J.E. and Hubbard D.E., *Sensors and Actuators, B*, 13 (1994).
14. Izutsu K. and Yamamoto H., *Analytical Sciences*, **12**, 905 (1996).
15. Abu Irhayem E., Elżanowska H., Jhas A., Skrzynecka B. and Birss V.I.,*J. Electroanal. Chem.*, **538**, 153 (2002).
16. Conway B.E., *J. Electrochem. Soc.*, **138**, 1539 (1991).
17. Bardin M., Loheac P., Petit M., Plichon V. and Richard N., *New J. Chem.*, **19**, 59 (1995).
18. Conway B.E., Birss V. and Wojtowicz J., *J. Power Sources*, **66**, 1 (1997).
19. Burke L.D. and Whelan D.P., *J. Electroanal. Chem.*, **162**, 121 (1984).
20. Burke L.D., Mulcahy J.K. and Whelan D.P., *J. Electroanal. Chem.*, **163**, 117 (1984).
21. Burke L.D. and Scannel R.A., *J. Electroanal. Chem.*, **175**, 119 (1984).

22. Pickup P.G. and Birss V.I., *J. Electroanal. Chem.*, **220**, 83 (1987).
23. Pickup P.G. and Birss V.I., *J. Electroanal. Chem.*, **240**, 171 (1988).
24. Pickup P.G. and Birss V.I., *J. Electroanal. Chem.*, **240,** 185 (1988).
25. Pickup P.G. and Birss V.I., *J. Electrochem. Soc.*, **135**, 41 (1988).
26. Pickup P.G. and Birss V.I., *J. Electroanal. Chem.*, **135**, 126 (1988).
27. Birss V.I., Elżanowska H. and S. Gottesfeld, *J. Electroanal. Chem.*, **318**, 327 (1991).
28. Elżanowska H. and Birss V.I., *J. Appl. Electrochem.*, **23**, 646 (1993).
29. Elżanowska H. and Birss V.I., *Polish J. Chem.*, **24**, 38 (1996).
30. Birss V.I., Bock C., and Elżanowska H., *Can. J. Chem.*, **75**, 1687 (1997).
31. H. Elżanowska, J. Segal and V.I. Birss, *Electrochim. Acta*, **44**, 4515 (1999).
32. Birss V.I., Andreas H., Serebrennikova I. and Elżanowska H., *Electrochem. and Solid State Letters*, **2**, 326 (1999).
33. Andreas H., Elżanowska H., Serebrennikova I. and Birss V.I., *J. Electrochem. Soc.*, **147**, 4598 (2000).
34. Bock C. and Birss V.I., *J. Electroanal. Chem.*, **475**, 20 (1999).
35. Bock C. and Birss V.I., *J. Electrochem. Soc.*, **146**, 1766 (1999).
36. Woods R., *J. Electroanal.Chem.*, **49**, 217 (1974).
37. Elzanowska H., Abu-Irhayem E., Skrzynecka B. and Birss V.I., *Electroanalysis*, **16**, 1 (2004).
38. Czerwinski A. and Zelazowska M., *J. Electroanal. Chem.*, **410**, 55 (1996).
39. Czerwinski A. and Zelazowska M., *J. Power Sources*, **64**, 29 (1997).
40. Czerwinski A., Zelazowska M., Grden M., Kuc K., Milewski J.D., Nowacki A., Wojcik G. and Kopczyk M., *J. Power Sources,* **85**, 49 (2000).
41. Adzic R., Yeager E. and Cahan B.D., *J. Electrochem. Soc.*, **121**, 474 (1974).
42. Birss V.I. and Shevalier M.T., *J. Electrochem. Soc.*, **137**, 2643 (1990).
43. Zeng X. and Bruckenstein S., *J. Electrochem. Soc.*, **146**, 2549 (1999).
44. Kortenaar M.V., Vente J.F., Ijdo D.J.W., Müller S. and Kötz R., *J. Power Sources*, **56**, 51 (1995).